Endonuclease FEN1 Coregulates ERα Activity and Provides a Novel Drug Interface in Tamoxifen-Resistant Breast Cancer

Koen D. Flach[1,2,3], Manikandan Periyasamy[4], Ajit Jadhav[5], Dorjbal Dorjsuren[5], Joseph C. Siefert[1,2], Theresa E. Hickey[6], Mark Opdam[7], Hetal Patel[4], Sander Canisius[8], David M. Wilson III[9], Maria Donaldson Collier[1,2], Stefan Prekovic[1,2], Marja Nieuwland[10], Roelof J.C. Kluin[10], Alexey V. Zakharov[5], Jelle Wesseling[7], Lodewyk F.A. Wessels[2,8], Sabine C. Linn[7], Wayne D. Tilley[6], Anton Simeonov[5], Simak Ali[4], and Wilbert Zwart[1,2,11]

ABSTRACT

Estrogen receptor α (ERα) is a key transcriptional regulator in the majority of breast cancers. ERα-positive patients are frequently treated with tamoxifen, but resistance is common. In this study, we refined a previously identified 111-gene outcome prediction-classifier, revealing FEN1 as the strongest determining factor in ERα-positive patient prognostication. FEN1 levels were predictive of outcome in tamoxifen-treated patients, and FEN1 played a causal role in ERα-driven cell growth. FEN1 impacted the transcriptional activity of ERα by facilitating coactivator recruitment to the ERα transcriptional complex. FEN1 blockade induced proteasome-mediated degradation of activated ERα, resulting in loss of ERα-driven gene expression and eradicated tumor cell proliferation. Finally, a high-throughput 465,195 compound screen identified a novel FEN1 inhibitor, which effectively blocked ERα function and inhibited proliferation of tamoxifen-resistant cell lines as well as *ex vivo*–cultured ERα-positive breast tumors. Collectively, these results provide therapeutic proof of principle for FEN1 blockade in tamoxifen-resistant breast cancer.

Significance: These findings show that pharmacologic inhibition of FEN1, which is predictive of outcome in tamoxifen-treated patients, effectively blocks ERα function and inhibits proliferation of tamoxifen-resistant tumor cells.

Introduction

Approximately 70% of all breast tumors are of the luminal subtype and their proliferation often depends on the activity of estrogen receptor α (ERα). Following ERα activation by estradiol (E2), a transcriptional complex is formed, initiated by steroid receptor coactivator (SRC) p160 recruitment, driving ERα-mediated transcription and cell proliferation programs (1).

Tamoxifen is often used in patients with ERα-positive breast cancer, where it competitively blocks E2-binding, preventing coactivator-binding pocket formation and inhibiting cell proliferation (2). P160 member SRC3 (NCOA3, AIB1) is frequently amplified in breast tumors and correlates with a poor outcome after tamoxifen treatment (3).

Previously, we assessed the genome-wide chromatin binding landscape of all three p160 coactivators in MCF7 breast cancer cells (4). Preferentially enriched chromatin-binding sites for each of the p160 family members were found, where genomic regions preferentially bound by SRC3 were uncovered proximal to 111 E2-responsive genes. Based on these genes, we developed a prognostic classifier for outcome after tamoxifen treatment. Which individual genes in the original classifier are critically involved in the observed clinical outcome remain elusive.

Besides recruitment of classic coregulators such as p160 proteins, DNA-modulating and DNA repair factors can also be recruited by ERα (5), as recently shown for APOBEC3B (6). APOBEC3B induces C-to-U deamination at ERα-binding regions, leading to uracil DNA glycosylase (UNG) recruitment and ultimately to phosphorylation of H2AX at Serine 139 (γH2AX; ref. 6). While in theory, the resulting UNG-mediated region of DNA that contains neither a purine nor a pyrimidine (abasic site) can be repaired by the base excision repair (BER) pathway (7), the exact interplay of BER proteins with ERα function remains unclear.

FEN1 is a member of the RAD2 nuclease family and cleaves overhanging flap structures that arise during lagging-strand DNA synthesis (e.g., Okazaki fragments; ref. 8) or long-patch BER, yielding a single-stranded DNA nick, which can be ligated by DNA-ligase

[1]Division of Oncogenomics, The Netherlands Cancer Institute, Amsterdam, the Netherlands. [2]Oncode Institute, the Netherlands. [3]Division of Gene Regulation, The Netherlands Cancer Institute, Amsterdam, the Netherlands. [4]Department of Surgery and Cancer, Imperial College London, London, United Kingdom. [5]National Center for Advancing Translational Sciences, NIH, Bethesda, Maryland. [6]Dame Roma Mitchell Cancer Research Laboratories, Adelaide Medical School, Faculty of Health Sciences, University of Adelaide, Adelaide, South Australia. [7]Division of Molecular Pathology, The Netherlands Cancer Institute, Amsterdam, the Netherlands. [8]Division of Molecular Carcinogenesis, The Netherlands Cancer Institute, Amsterdam, the Netherlands. [9]Laboratory of Molecular Gerontology, Intramural Research Program, National Institute on Aging, NIH, Baltimore, Maryland. [10]Genomics Core Facility, The Netherlands Cancer Institute, Amsterdam, the Netherlands. [11]Laboratory of Chemical Biology and Institute for Complex Molecular Systems, Department of Biomedical Engineering, Eindhoven University of Technology, Eindhoven, the Netherlands.

Note: Supplementary data for this article are available at Cancer Research Online (http://cancerres.aacrjournals.org/).

Current address for D.M. Wilson III: Biomedical Research Institute, Hasselt University, Hasselt, Belgium.

Corresponding Author: Wilbert Zwart, The Netherlands Cancer Institute, Plesmanlaan 121, Amsterdam 1066CX, The Netherlands. Phone: 312-0512-2101; Fax: 312-0512-2027; E-mail: w.zwart@nki.nl

Cancer Res 2020;80:1914–26

doi: 10.1158/0008-5472.CAN-19-2207

1 (7). FEN1 deficiency predisposes to tumor development and FEN1 is upregulated in numerous tumor types, including breast cancer (9). Although endogenous ERα/FEN1 interactions have not been reported, incubation of immobilized FLAG-tagged ERα with MCF7 nuclear extracts did identify FEN1 as an ERα-associating protein (10). Even though endogenous FEN1 was described as recruited to the TFF1 promoter and FEN1 knockdown resulted in reduced TFF1 mRNA expression (10), it remains unknown whether FEN1 regulates estrogen responsiveness in a genome-wide manner or by which mechanism. In addition, FEN1 levels correlate negatively with overall survival in patients with breast cancer (11), but whether ERα status is the driving force behind this clinical observation remains unclear.

Here, we demonstrate that FEN1 dictates the transcriptional activity of ERα by facilitating the formation of a functional transcriptional complex. Perturbation of FEN1 function results in deregulated ERα-responsive gene expression and reduced cell proliferation. FEN1 additionally regulates ERα's activity by stabilizing chromatin interactions after activation. We show that FEN1 is a predictive marker of tamoxifen response in patients with ERα-positive breast cancer, playing a key role in ERα-driven cell proliferation. A novel small-molecule inhibitor of FEN1 blocked proliferation of tamoxifen-resistant cell lines as well as primary ERα-positive tumor explants, yielding a novel therapeutic lead in the clinical management of tamoxifen resistance. Cumulatively, we present a pioneering proof of concept that spans from gene classifier and causal gene identification, to molecular mechanism, novel drug development, and validation in ERα-positive breast cancer.

Materials and Methods

Colony formation

For the colony formation assay 2,500 cells/well were plated in 48-well format in appropriate culture medium. After attachment of cells to the bottom of the well, the FEN1 inhibitor was administered and when appropriate 100 nmol/L 4OH-tamoxifen was added. After 7 days, cells were fixed with 100% of methanol and cells were stained with 0.2% crystal violet. For quantification, the crystal violet was dissolved in 10% acetic acid and the optical density was measured at 560 nm.

Cell culture

MCF7, T47D, MDA-MB-231, and CAL120 cells were cultured in DMEM medium in the presence of 10% FBS and antibiotics (penicillin, streptavidin). TAMR and MCF7-T cells were cultured in phenol-red-free DMEM containing 5% charcoal-treated serum (CTS; HyClone), 2 mmol/L of -glutamine, antibiotics, and 100 nmol/L 4OH-tamoxifen. BT20 cells were cultured in MEM in the presence of 10% FBS and antibiotics. For hormone-deficient conditions, cells were deprived of hormone for 72 hours, by culturing in phenol-red-free DMEM containing 5% CTS, antibiotics, and supplemented with L-glutamine, prior to hormone treatment. Hormone treatments consisted of solvent DMSO, 10 nmol/L of estradiol, 100 nmol/L of 4OH-tamoxifen, or 100 nmol/L of fulvestrant. All cell lines were tested for *Mycoplasma* every 3 months and were genotyped for authenticity by Applied Biosystems. MCF7, T47D, and MDA-MB-231 were purchased from ATCC. CAL120 and BT20 cells were kindly provided by R.L. Beijersbergen (Division of Carcinogenesis, The Netherlands Cancer Institute, Amsterdam, the Netherlands). MCF7-T and TAMR (tamoxifen-resistant MCF7 derivatives (12, 13) were kindly provided by Kenneth P. Nephew (Medical Sciences Program, Indiana University School of Medicine, Bloomington, Indiana) and R.I. Nicholson (Department of Molecular Biology & Genetics, Cornell University, Ithaca, NY).

RNA-seq

Cells transfected with siFEN1 or siControl were hormone deprived and treated for 6 hours with E2 or vehicle. Four biological replicates were used per condition. Read counts were mapped using Salmon v0.14.1 and differential expression (DE) was performed using DESeq2 with an FDR (adjusted P value) < 0.05. Median of ratio normalization was performed across all samples and differentially expressed genes were identified between E2 versus vehicle and siFEN1 versus siControl conditions. The overlap of these two sets was defined as the FEN1 and E2-responsive genes. Gene set enrichment analysis (GSEA) was performed with clusterProfiler, using all genes ranked by ($\log_2$-fold change $\times$ -$\log_{10}P$).

Transient transfections of siRNA and plasmids

For knockdown experiments, 25 nmol/L of single or pooled duplexes of siRNA against FEN1 (Dharmacon MU-010344-01) or a nontargeting control pool (Dharmacon, D-001206-14-20) were transfected with Dharmafect according to manufacturer's protocol. The expression plasmids pShuttle-FEN1hWT (wild-type FEN1) and pShuttle-FEN1DA (D181A point mutant) were kindly provided by Sheila Stewart (Addgene plasmid, catalog nos. 35027 and 35028; ref. 14) and cells were transfected with polyethylenimine. When appropriate cells were hormone-deprived for 24 hours prior to siRNA transfection or overexpression and further hormone deprived for 48–72 hours.

Chromatin immunoprecipitation and formaldehyde-assisted isolation of regulatory elements

Chromatic immunoprecipitation (ChIP) experiments were performed as described previously (4) with the following modifications. Three to 10 micrograms of antibody was prebound overnight to protein A Dynabeads magnetic beads (Invitrogen). The magnetic bead-chromatin complexes were harvested and washed 10 times with RIPA buffer [50 mmol/L HEPES (pH 7.6), 1 mmol/L EDTA, 0.7% Na deoxycholate, 1% NP-40, 0.5 M LiCl]. Antibodies used were anti-ERα (sc-543), anti-FOXA1 (sc-6554), anti-BRG1 (sc-10768), and anti-PARP1 (sc-1561) from Santa Cruz Biotechnology and anti-RNA polymerase II (ab5408), anti-XRCC1 (ab9147) from Abcam. In **Fig. 4**, publically available ChIP-seq data was used; ERα (15) and γH2AX (GSE57426; ref. 6). Formaldehyde-assisted isolation of regulatory elements (FAIRE) was performed as described previously (16). ChIP-seq and FAIRE-seq data can be found on GEO: GSE95302.

Solexa ChIP and FAIRE sequencing and enrichment analysis

ChIP DNA was amplified as described previously (17). Sequences were generated by the Illumina Hiseq 2000 genome analyser (using 51 or 65 bp reads), and aligned to the Human Reference Genome (assembly hg19, February 2009). Peak calling over input was performed using MACS peak caller (18) version 1.3.7.1 and DFilter (19), only considering peaks shared by both peak callers. For **Figs. 2B** and **4C**, all ERα-binding regions after 45 minutes of estradiol as published before (15) were used. Details on the number of reads obtained and the percentage of reads aligned can be found below. ChIP-seq and FAIRE-seq data can be found on GEO: GSE95302.

Sequencing snapshots and Heatmaps

ChIP-seq data snapshots were generated using the Integrative Genome Viewer IGV 2.2 (www.broadinstitute.org/igv/). Heatmaps were generated using Seqminer, with default settings (20).

mRNA-qPCR expression and ChIP-qPCR

For mRNA expression, cells were treated with vehicle or 100 nmol/L of FEN1 inhibitor, after which, total RNA was collected by phenol-chloroform extraction. cDNA was made with a Superscript III RT Kit (Invitrogen) using manufacturer's protocols, after which, qPCR was performed. *TBP* and *UBC* were used as housekeeping genes. For ChIP, DNA-protein interactions were harvested with ChIP and obtained DNA regions were used after immunoprecipitation. qPCR was performed with SYBR Green (Applied Biosystems) on a Roche LightCycler 480 Real-Time PCR System using standard protocols. A negative region near the cyclin D1 (CCND1) promoter was used as a negative control. When appropriate, an additional negative control primer (Neg 2) was taken along. Primers are described below.

Primers cDNA

Homo sapiens trefoil factor 1 (TFF1): forward (FWD) ATCGACGTCCCTCCAGAAGA; reverse (REV) TGGGACTAATCACCGTGCTG; X-box binding protein 1 (XBP1): FWD GGGAAGGGCATTTGAAGAAC, REV ATGGATTCTGGCGGTATTGA; retinoic acid receptor alpha (RARA): FWD GACCAGATCACCCTCCTCAA, REV GTCCGAGAAGGTCATGGTGT; TATA box binding protein (TBP): FWD GTTCTGGGAAAATGGTGTGC, REV GCTGGAAAACCCAACTTCTG; ubiquitin C (UBC): FWD ATTTGGGTCGCAGTTCTTG, REV TGCCTTGACATTCTCGATGGT.

Primers ChIP

cyclin D1 (CCND1; Neg 1): FWD TGCCACACACCAGTGACTTT, REV ACAGCCAGAAGCTCCAAAAA; Homo sapiens trefoil factor 1 (TFF1): FWD TGGTCAAGCTACATGGAAGG, REV CCATGGGAAAGAGGGACTTT; growth regulation by estrogen in breast cancer 1 (GREB1): FWD CACTTTGAGCAAAAGCCACA, REV GCTGCGGCAATCAGAAGTAT; X-box binding protein 1 (XBP1): FWD GGTCACAGGCTGCCAAGTAT, REV AGCCCCAGTTATGGCGTAAT; retinoic acid receptor alpha (RARA): FWD CTCAGGACAGGGCAAGAGTG, REV AAGCCACTCCAAGGTAGGTG; Negative control 2 (Neg 2): FWD TGGCCCTTGATACTGGAGTC, REV GACATCCAAGGCAAGATGGT; PDZ Domain Containing 1 (PDZK1): FWD AGGCCCAGCAAAGACAAATG, REV AAACCACAGGCTGAGGACTG.

Coimmunoprecipitation

Immunoprecipitations were performed as described previously (21). MCF7 cells were lysed in RIPA whole-cell lysate buffer containing protease inhibitors. Lysates were precleared by incubating with preclearing beads (Immunocruz, Santa Cruz Biotechnology) at 4°C for 2 hours. Five micrograms of ERα antibody (ER HC20) was incubated with agarose beads (Immunocruz, Santa Cruz Biotechnology) for 2 hours at 4°C. Agarose beads conjugated with ERα antibody were washed three times with ice-cold PBS and resuspended in PBS and transferred to the precleared lysates for overnight incubation. Following incubation, beads were washed six times in ice-cold PBS and resuspended in 2× sample buffer (Sigma, 0.125 mol/L Tris-HCL at pH 6.8, 4% SDS, 20% glycerol, 10% β-mercaptoethanol and 0.004% bromophenol blue) and heated at 95°C for 10 minutes, and then analyzed by Western blot analysis. The following antibodies were used for IP: anti-ERα (sc-543) from Santa Cruz Biotechnology, and for Western blot analysis; anti-ERα (6F11) from Leica Biosystems, anti-AIB1 (BD Biosciences, catalog no. 611105) and anti-Lamin A/C (sc-7292), and anti-FEN1 (sc-28355) from Santa Cruz Biotechnologies.

Western blot analysis

Cells were lysed with 2× Laemmli buffer (containing 1:500 Na3VO4, 1:10 NaF, 1:13 β-glutamate, 1:100 protease inhibitors, 1:100 phosphatase inhibitors). Western blot analysis samples contained 10% DTT and 4% bromophenol blue and were incubated for 5 minutes at 95°C. Samples were run on 10% SDS-PAGE gel and transferred to nitrocellulose membranes. The following primary antibodies were used: anti-p300 (sc-585), anti-FOXA1 (sc-6554), anti-ERα (sc-543), and anti-FEN1 (sc-13051) from Santa Cruz Biotechnology, anti-RNA polymerase II (ab5408) from Abcam and 1:10,000 actin from Millipore (MAB1501R). The following secondary antibody was used: 1:10,000 LI-COR Odyssey IRDue. Membranes were scanned and analyzed with Odyssey V3.0.

Patient cohorts

The discovery cohort has been used and described previously (22). In short, ERα-positive patients that received tamoxifen in the adjuvant setting, but did not receive adjuvant chemotherapy, were selected from The Netherlands Cancer Institute–Antoni van Leeuwenhoek Hospital (NKI–AVL; Amsterdam, the Netherlands). Distant metastases were regarded as failure to treatment and used as events. RNA was hybridized on 44 K oligomicroarrays, as described previously (23). The median IHC-score and mRNA expression value was chosen as the cut-off point.

The validation cohort has been described before (IKA trial, 1982–1994; ref. 24). In short, ERα-positive patients (no adjuvant chemotherapy) were randomized between 1-year tamoxifen versus no adjuvant therapy. After 1 year, a second randomization was performed; 2 additional years of tamoxifen or to stop further treatment. Further patient characteristics and clinical outcome of the original study group (1,662 patients) have been described before (25). For 739 patients, sufficient tumor material for IHC was available (25). The median IHC-score value was chosen as the cut-off point.

IHC

Tissue microarrays (TMA) were constructed using formalin-fixed paraffin embedded tumor blocks. A total of three (0.6 mm) cores per tumor were embedded in the TMA. TMAs were stained for FEN1 and hematoxylin and eosin with the ULTRA BenchMark IHC/ISH Staining Module of the NKI (Amsterdam, the Netherlands). Antibody used was anti-FEN1 (sc-13051) from Santa Cruz Biotechnology. The percentage of FEN1-positive invasive tumor cells was scored. One TMA was scored independently in a blinded manner by a second observer to calculate interobserver variability ($\kappa = 0.708$). The interobserver variability was analyzed using the (weighted) Cohen kappa coefficient.

For *ex vivo* tumor cultures, tissue sections were incubated with a Ki67 primary antibody (MIB1 1:400; DAKO M7240) at 4°C overnight followed by detection using a biotinylated anti-mouse secondary antibody at 1:400 dilution (DAKO E0433) for 30 minutes followed by incubation with horseradish peroxidase–conjugated streptavidin (DAKO P0397). Visualization of immunostaining was performed using 3,3-diaminobenzidine (Sigma D9015).

Statistical analysis

Prediction analysis for microarrays (PAM; ref. 26) was performed to determine the minimum number of genes required to attain accurate separation of good and poor survival. Here, good and poor survival were defined on the basis of whether or not a distant metastasis occurred within 5 years. The number of genes was selected such that the AUC was optimized in a 10-fold cross-validation. Subsequently,

Lasso-penalized logistic regression (27) was used to obtain a robust selection of the best performing genes across two cohorts (28, 29). To this end, 1,000 cross-validation analyses were performed for each cohort to select gene subsets optimizing the AUC. Genes were then ranked according to how many times they were part of the optimal gene set in either of the two cohorts. Finally, the previously determined optimal number of genes were selected starting from the highest ranked gene.

Pearson correlation coefficient was used to assess the correlation between relative FEN1 mRNA levels and FEN1 IHC scores. Survival curves were constructed using the Kaplan–Meier method and compared using log-rank test. Unadjusted and adjusted Cox proportional hazard regression analyses were performed; for the discovery-cohort the covariates age (<60 vs. ≥60), diameter of the tumor (≤20 mm vs. 20–50 mm vs. >50 mm), tumor grade (grade 1 vs. grade 2 vs. grade 3), and the number of affected lymph nodes (negative vs. 1–3 vs. ≥4); and for the validation-cohort the covariates age (< 65 vs. ≥ 65), grade (grade 1–2 vs. grade 3), tumor stage (T1-T2 vs. T3-T4), HER2 status (negative vs. positive), PgR status (negative vs. positive). In the validation-cohort, all analyses were stratified for nodal status (negative vs. positive) because lymph node positive patients, after 1989, skipped the first randomization and all received 1 year of tamoxifen. A P value <0.05 was considered as a significant result and FEN1 levels were used a binary factor to assess the interaction with adjuvant treatment. A two-tailed Student t test was performed when appropriate.

Immunofluorescence

Immunofluorescence analysis was performed as described previously (6). Briefly, hormone-deprived MCF7 cells were cultured on glass coverslips before the addition of 10 nmol/L E2. In addition, cells were pretreated with 100 nmol/L of FEN1 inhibitor as appropriate. Cells were fixed with 4% paraformaldehyde for 10 minutes and permeabilized with 0.2% Triton X-100. Used primary antibody was γH2AX (05-636, Millipore) and for secondary Alexa fluor 488 (Invitrogen) was used. ToPro (Invitrogen) nuclear dye was used to visualize nuclei. Images were acquired using a Carl Zeiss confocal microscope using LSM 510 image browser. Images were analyzed using Fuji Image J (NIH, Maryland, USA) and Cell Profiler (Broad Institute, Massachusetts, USA) to quantify number of foci per cell.

Primary *ex vivo* tumor cultures

Breast tumor samples and relevant clinical data were obtained from women undergoing surgery at the Burnside Private Hospital, Adelaide, South Australia, with written informed consent. This study was approved by the University of Adelaide Human Research Ethics Committee (approval numbers: H-065-2005, H-169-2011). Following surgery, excised tissue samples were cultured *ex vivo* as described previously (30, 31). Briefly, tumor pieces were cultured on gelatin sponges in full medium containing a vehicle, FEN1 inhibitor (200 nmol/L) or, when enough material was present, tamoxifen (2 μmol/L). After 3 to 6 days, tissue was fixed in 4% formalin in PBS at 4°C overnight and subsequently processed into paraffin blocks. Slices (2 μm) were stained with hematoxylin and eosin or Ki67 and examined by a pathologist to confirm the presence/proportion of tumor cells. Tumor slides were scored by a pathologist for the percentage of Ki67-positive tumor cells.

FEN1 inhibitor screen

The previously reported nonradioactive FEN1 activity assay (32) was combined with a quantitative high throughput screen (qHTS; ref. 33) and implemented on a fully integrated robotic system (34), utilizing a large-scale chemical library arrayed in qHTS-formatted 1,536-well based plates (35). A total of 465,195 compounds were tested. Automated large-scale curve fitting and classification of curve types were determined (33). Using this classification, 3,543 compounds were considered inconclusive or weak inhibitors due to either lower quality curves or moderate inhibition. Another 1,123 compounds demonstrated a dose-dependent increase in fluorescent signal, but were regarded as likely inactive due to suspected autofluorescence, which was observed in the initial background read. A total of 2,485 compounds were categorized as active FEN1 inhibitors and as part of the NIH Molecular Libraries Program (https://commonfund.nih.gov/molecularlibraries) profiled for their effect in over 150 biochemical and cell-based assays. Furthermore, cheminformatics filters were applied to the chemical library to annotate compounds for their reactivity (36). See also PubChem AID: 488816, 588795, and 720498.

Results

FEN1 levels correlate with breast cancer patient survival after tamoxifen treatment

In a previous report, we identified 111 genes that predict outcome in tamoxifen-treated patients with ERα-positive breast cancer (4). To reveal drivers causally involved in the observed patient outcome, we refined the gene signature to identify a minimal set of genes without losing predictive capacity (**Fig. 1A**). Computationally minimizing the 111-gene classifier by PAM (26) and Lasso-penalized logistic regression (27) in two independent cohorts of tamoxifen-treated patients (28, 29) illustrated that the classifier could be reduced to four genes before losing its stratification potential: FEN1, MCM2, STARD13, and HBP1 (**Fig. 1A**). Validation of the four genes in the METABRIC dataset (37) demonstrated that only FEN1 was significant by multivariate analysis in ERα-positive, but not ERα-negative cases (Supplementary Fig. S1A), suggesting FEN1 is selectively associated with outcome in ERα-positive breast cancer.

To assess the clinical impact of both FEN1 mRNA and protein levels as a single-gene classifier on survival, we first used samples of ERα-positive cases that received adjuvant tamoxifen (Discovery-cohort; ref. 22), using microarray-based (mRNA) and IHC-based (IHC) FEN1 expression ranging from 0% to 100% positive tumor cells (**Fig. 1B**), which correlated with FEN1 mRNA levels (Pearson correlation coefficient = 0.58; **Fig. 1C**). For both mRNA and IHC, the median was used to stratify patients into "Low" and "High" FEN1 groups (**Fig. 1D**). FEN1 mRNA (HR: 2.46; $P = 0.006$; **Fig. 1E**; Supplementary Table S1) and protein (HR: 2.05; $P = 0.041$; **Fig. 1F**; Supplementary Table S1) expression were associated with distant metastasis-free survival (DMFS), with high FEN1 levels correlating with a poor survival.

To validate these findings in an independent cohort and to further investigate whether FEN1 associates with disease progression (prognostic classifier) or whether its levels are informative for treatment response (predictive classifier), we utilized tissue from a cohort where patients were randomized between tamoxifen or no adjuvant endocrine therapy (validation cohort; ref. 24). As this cohort contains a matched non-tamoxifen–treated group, it can provide an extra level of evidence with regards to predictive potential that is not available from other tamoxifen cohorts that lack a non-endocrine–treated control group (38).

In this validation cohort, FEN1 was associated with recurrence-free survival (RFS) in ERα-positive patients ($n = 389$; HR = 1.90; $P = 0.002$; **Fig. 1G**), also after multivariate correction for age, tumor grade, tumor stage, HER2, PgR, and lymph node status (adjusted HR = 1.58; $P = 0.047$; Supplementary Table S1), which was successfully confirmed

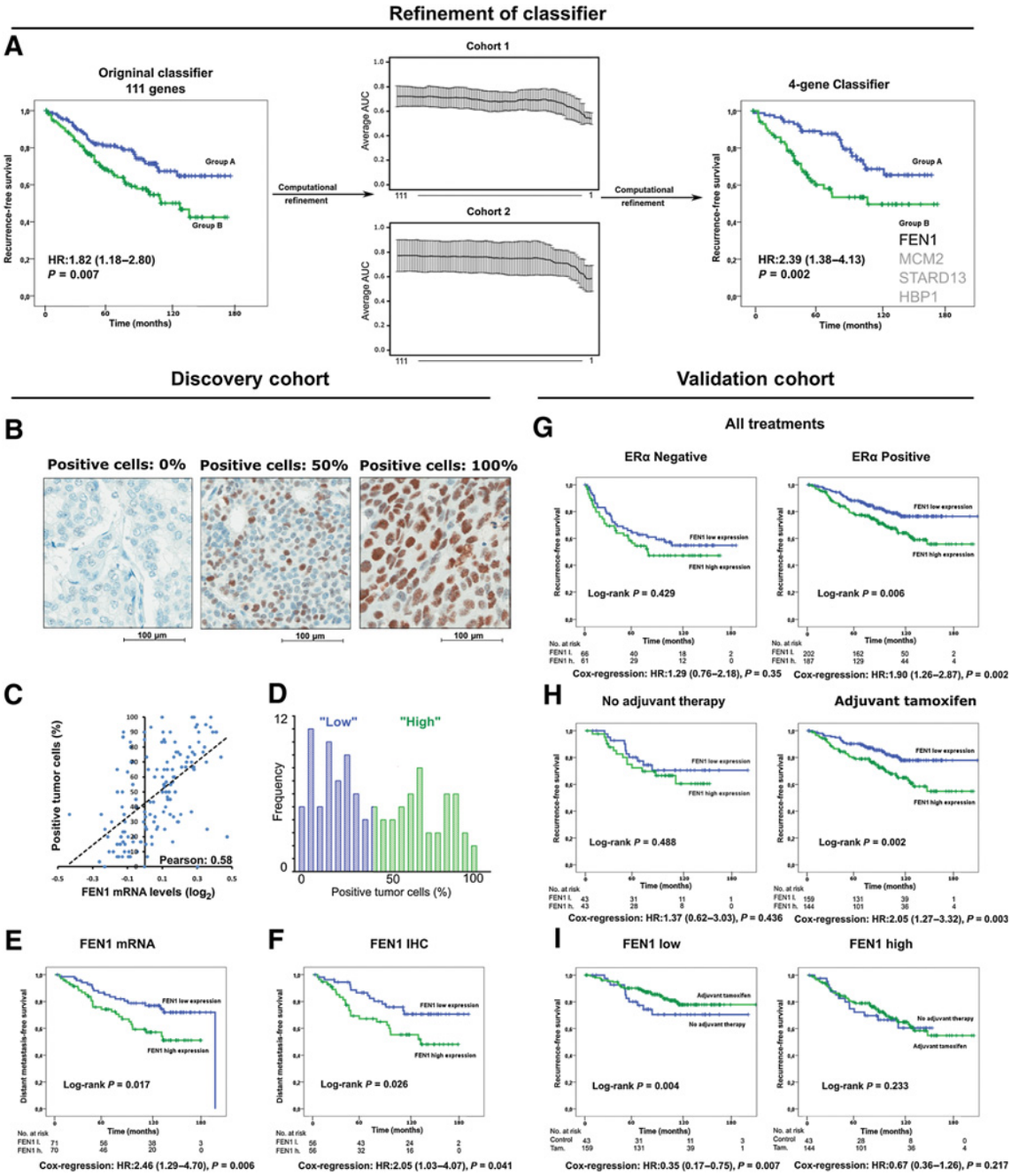

Figure 1.

FEN1 levels as predictive marker for tamoxifen response of patients with breast cancer. **A,** Computational refinement of 111-gene classifier toward 4-gene classifier of FEN1, MCM2, HBP1, and STARD13. PAM and Lasso-penalized logistic regression was performed to determine the minimum number of genes without affecting performance. Left, RFS of patients categorized according to 111-gene classifier. Cox regression is shown. Middle, stepwise minimization of the 111-genes with corresponding average AUC in two cohorts. Right, RFS of patients categorized according to 4-gene classifier. Cox regression is shown. See also Supplementary Fig. S1A. **B,** Three representative IHC tumor cores, staining negative (0%), intermediate (50%), or entirely positive (100%) for FEN1. Scale bar, 100 µm. **C,** Scatterplot showing FEN1 mRNA levels (*x*-axis) related to FEN1 protein expression (% tumor cells, *y*-axis), from the same tumor samples. Dotted line, trend line. Pearson correlation coefficient = 0.58. **D,** Bar graph showing the individual IHC-scores for all tumor samples. Tumors were stratified in "Low" (IHC-score ≤ 36%) or "High" (IHC-score > 36%) FEN1. **E,** DMFS of tamoxifen-treated patients categorized according to FEN1 mRNA levels. Log-rank and Cox regression are shown. See also Supplementary Table S1. **F,** As in **E**, but now patients were categorized according to FEN1 IHC-score. **G,** Randomized clinical trial: RFS of patients stratified by ERα-status and categorized according to FEN1 IHC-score. Log-rank and Cox regression are shown. See also Supplementary Table S1 and Supplementary Fig. S1B. **H,** As in **G**, but now patients were stratified for adjuvant therapy (none or tamoxifen) and categorized according to FEN1 IHC-score. See also Supplementary Table S1. **I,** As in **G,** but now patients were stratified for FEN1 IHC-score and categorized according to adjuvant therapy (none or tamoxifen). See also Supplementary Table S1.

in the METABRIC dataset (Supplementary Fig. S1A and S1B). No association was found between FEN1 levels and RFS in patients with ERα-negative breast cancer ($n = 127$; HR = 1.29; $P = 0.35$; **Fig. 1G**; Supplementary Fig. S1B). To make sure, this difference in significant association with RFS was not due to the difference in patient numbers, we downsampled the ERα-positive patients group to $n = 127$ (matching the ERα-negative group) showing that FEN1 levels were still significantly associated with RFS (log-rank $P = 0.028$; Cox regression HR = 2.19; $P = 0.033$; Supplementary Fig. S1C). Furthermore, high FEN1 significantly correlated with poor outcome in tamoxifen-treated patients (HR = 2.05; $P = 0.003$), but not for patients not receiving endocrine therapy (HR = 1.37; $P = 0.436$; **Fig. 1H**; Supplementary Table S1).

Next, we stratified patients according to FEN1 levels and categorized by tamoxifen treatment (**Fig. 1I**). Patients with high FEN1 did not benefit from tamoxifen (HR = 0.67; $P = 0.217$), while tamoxifen-treated patients with low FEN1 had a better survival as compared with those who did not receive adjuvant tamoxifen (HR = 0.35; $P = 0.007$), also after multivariate correction (high FEN1 adjusted HR = 0.67, $P = 0.213$; low FEN1 adjusted HR = 0.39; $P = 0.015$; Supplementary Table S1). The predictive potential of FEN1 levels was further illustrated by the interaction test between FEN1 levels and hormonal therapy status (HR = 2.19; $P < 0.001$; adjusted HR = 1.86; $P < 0.001$).

As the standard regimens of hormonal treatment for ERα-positive breast cancer have changed since the time of our validation cohort (e.g., 3 years of tamoxifen then vs. 2–3 years of tamoxifen followed by 5 years of an aromatase inhibitor now), we tested how FEN1 levels would perform in a cohort using more contemporary hormonal therapies (METABRIC). In patients treated with hormonal therapy, high FEN1 was associated poor disease-specific survival (HR = 2.09; $P < 0.001$), also after multivariate correction (adjusted HR = 1.83; $P < 0.001$; Supplementary Fig. S1D). In addition, we assessed whether the menopausal status of a patient would influence the performance of FEN1 as predictive biomarker, as in the clinical setting tamoxifen is predominately used in premenopausal women. Both in premenopausal (HR = 5.29; $P < 0.001$) and postmenopausal patients (HR = 1.79; $P < 0.001$), FEN1 levels were significantly associated with patient outcome, also after multivariate correction (premenopausal adjusted HR = 5.57, $P < 0.001$; postmenopausal adjusted HR = 1.62, $P < 0.001$; Supplementary Fig. S1E). Although significant in both menopausal states, the predictive potential of FEN1 appeared stronger in the premenopausal setting (HR5.57 vs. HR = 1.62).

In summary, FEN1 levels are not indicative of outcome in ERα-negative breast cancers, nor in ERα-positive disease in the absence of adjuvant endocrine therapy. Only in ERα-positive patients who were treated with tamoxifen, FEN1 levels were associated with poor outcome, rendering FEN1 a predictive marker for tamoxifen treatment response.

FEN1 is essential for ERα–chromatin interactions and transcriptional complex formation

FEN1 functions as a predictive marker for tamoxifen resistance in ERα-positive breast cancer. To determine whether FEN1 directly affects ERα activity, we tested if FEN1 is recruited to the ERα genomic complex. Based on coimmunoprecipitations in MCF7 cells, endogenous ERα and FEN1 interact in an estradiol-dependent fashion, which is comparable to the recruitment of SRC3 and p300 to the ERα complex (**Fig. 2A**). Strikingly, recruitment of SRC3 and p300 was greatly reduced upon FEN1 knockdown, implying a direct role for FEN1 in the formation of the ERα transcriptional complex (**Fig. 2A**). In addition, knockdown of FEN1 (Supplementary Fig. S2A; knockdown validation) abrogated ERα-chromatin interactions (**Fig. 2B** and **C**; Supplementary Table S2), which coincided with a loss of RNA polymerase II at these sites (Supplementary Fig. S2B). Of note, both motif enrichment (**Fig. 2D**) and genomic distribution (**Fig. 2E**) of siFEN1-affected ERα-chromatin interactions, demonstrate that siFEN1 results in the loss of "regular canonical ERα sites," and is unselective for specific motifs or genomic elements. In contrast to ERα, FOXA1 chromatin binding (**Fig. 2B** and **C**; Supplementary Fig. S2B) and chromatin accessibility (**Fig. 2F**) was not decreased by siFEN1, implicating FEN1 as a regulator of ERα-chromatin interactions downstream of FOXA1.

FEN1 impacts ERα-mediated transcription and cell proliferation

The above results demonstrate that FEN1 modulates ERα-chromatin interactions and transcription complex formation. Next, we assessed what the effect of FEN1 is on ERα-mediated transcription. RNA-seq demonstrated that upon E2 treatment, 1,298 genes were differentially expressed in siControl cells (**Fig. 3A**) while knockdown of FEN1 levels resulted in 218 differentially expressed genes (**Fig. 3B**). In this list of FEN1-responsive genes, a significant enrichment for E2-responsive genes was found (Fisher exact test; $P = 3.9e-25$), with around 24% (54 genes) overlapping with E2-responsive genes (**Fig. 3C**). GSEA of the E2 and FEN1 responsive genes showed a significant enrichment for the Hallmark Estrogen Response Late genes (**Fig. 3D**; full list Supplementary Fig. S3A).

As the Hallmark Estrogen Response Late genes were enriched in FEN1- and E2-responsive genes, we next assesed what the effect of this would be on ERα-mediated proliferation. FEN1 knockdown in MCF7 cells decreased ERα-mediated cell growth under DMSO and E2 conditions (**Fig. 3E**; siRNA deconvolution in Supplementary Fig. S3B), while FEN1 overexpression increased cell proliferation under these conditions (**Fig. 3F**). The observed decrease in cell proliferation after siFEN1 was validated in ERα-positive T47D cells (Supplementary Fig. S3C). Both in tamoxifen and fulvestrant (a selective estrogen receptor downregulator) treated cells, FEN1 knockdown did not result in substantial growth deffects (**Fig. 3E** and **F**). Moreover, FEN1 knockdown in ERα-negative MDA-MB-231 or CAL120 cells did not affect cell proliferation (**Fig. 3B**), implicating that the observed effects are mediated through ERα and not broadly related to the role of FEN1 in DNA replication (39). Cumulatively, we demonstrate that FEN1 impacts ERα-mediated transcription and cell proliferation.

FEN1 inhibition perturbs ERα activation and stability

Given FEN1's key role in modulating ERα activity, we hypothesized a FEN1 inhibitor could have therapeutic potential in treating ERα-positive breast cancer. Because FEN1 inhibitors have been developed before on a small scale (40, 41) but were not effective in breast cancer cell lines as single agent (42), other more-potent inhibitors could still be found. Therefore, we performed a small-molecule compound screen of 465,195 compounds, tested at six different concentrations, to identify novel inhibitors of FEN1's flap-cleaving activity. A previously reported nonradioactive FEN1 activity assay was used (32), in which a small DNA product containing fluorophore donor 6-TAMRA (6-Carboxytetramethylrhodamine) is cleaved and released by FEN1 from a DNA flap structure labeled with a fluorescent quencher (Black Hole Quencher 2), resulting in measurable fluorescence (**Fig. 4A**). A quantitative high throughput robotics screen (33) was performed on 465,195 compounds (35), identifying 2,485 active FEN1 inhibitors (**Fig. 4B**; Supplementary Fig. S4A). As part of the NIH Molecular Libraries Program (https://commonfund.nih.gov/molecularlibraries), these compounds have been profiled for their effect in >150

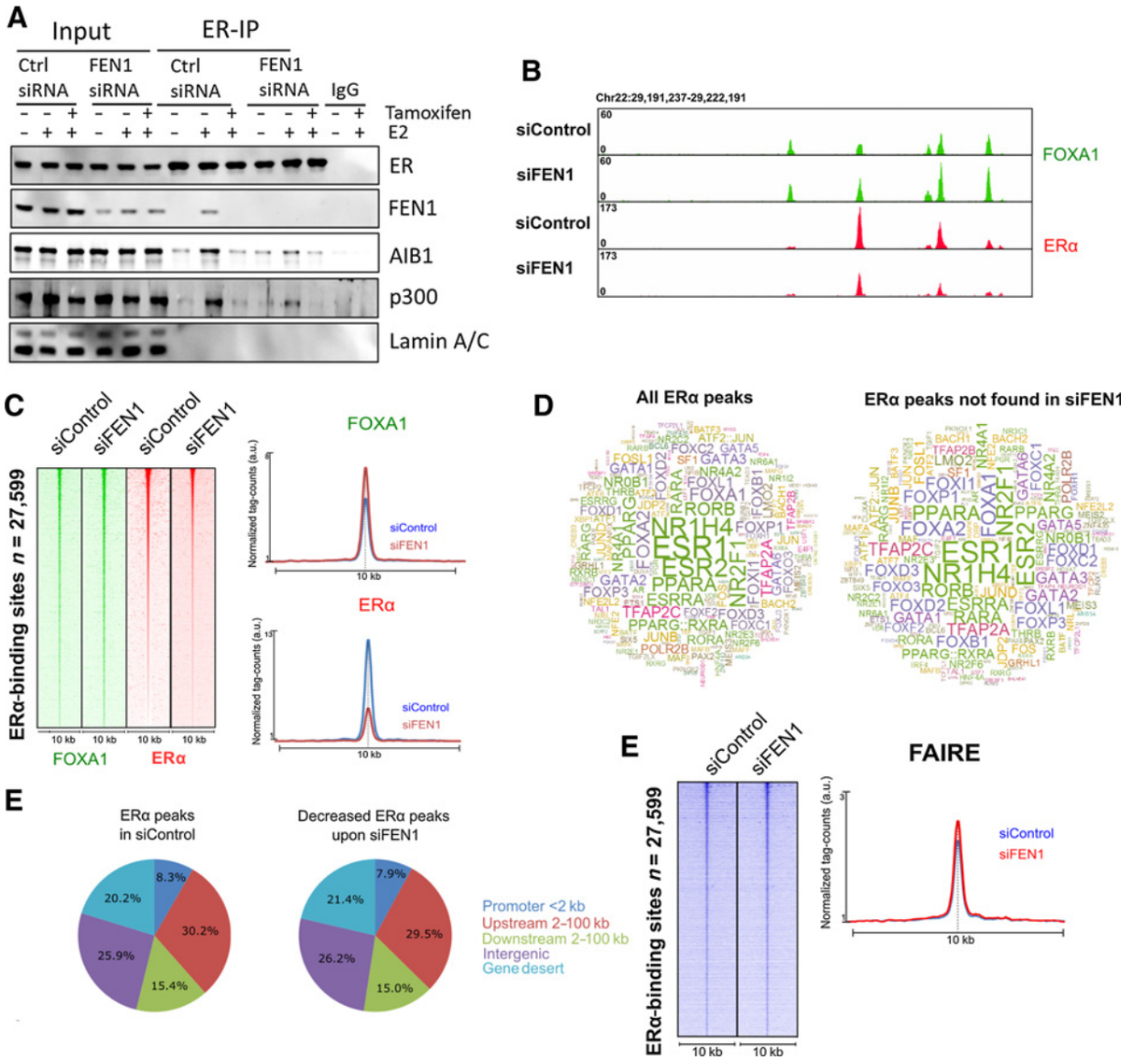

Figure 2.

FEN interacts with ERα and dictates ERα-chromatin interactions and complex formation. **A,** Coimmunoprecipitation analyses demonstrate E2-induced ERα/FEN1 interactions. Protein levels were determined for ERα, FEN1, SRC3, and negative control Lamin A/C. Cells were treated with (+) or without (−) E2 before immunoprecipitation of ERα or IgG. Shown is an example of two biological replicates. **B,** Genome browser snapshot at the XBP1 locus, illustrating FOXA1 (green) and ERα (red) binding events for siFEN1 and control. Genomic coordinates and tag count are indicated. See also Supplementary Fig. S2A–S2C. **C,** Left, heatmap visualizing binding events of FOXA1 (green) and ERα (red) at ERα-binding sites after FEN1 knockdown. All binding events are vertically aligned and centered on the ERα peak, with a 10 kb window. Peaks were sorted on ERα intensity. See also Supplementary Fig. S2A–S2C. Right, normalized tag counts of FOXA1 and ERα p300 are plotted, showing average signal intensity within a 10 kb window. **D,** ERα-binding motif analysis. SeqPos was used to identify binding motifs at all ERα-binding sites (siControl) and motifs at sites no longer identified in siFEN1. **E,** Genomic distribution of the same set of ERα-bindings sites described in **D**. **F,** As in **C**, but now binding events of FAIRE-seq are visualized. Shown is an example of two biological replicates.

biochemical and cell-based assays including DNA-repair and related screens (e.g., APE1, POLB, POLK, POLH, POLI, PCNA, DNA binding; Supplementary Fig. S4B; Supplementary Table S3). Furthermore, cheminformatics filters have been applied to annotate compounds for their reactivity (36). The selectivity profiling data and filters for reactive functional groups were used to triage the 2,485 active FEN1 inhibitors, and a set of 22 inhibitors was selected for further biological validation.

After testing the 22 hits on MCF7 cell proliferation, we continued with the three most-potent hits for further validation (Supplementary Fig. S4C) and selected FENi#2 (MLS002701801) as most potent and promising hit (**Fig. 4B**; Supplementary Fig. S4B and S4C; Supplementary Table S3).

Previously, it was shown that ERα cofactor APOBEC3B can induce C-to-U modifications and UNG recruitment at ERα binding sites, resulting in the induction of abasic regions of DNA, which regulate ERα-mediated transcriptional activity (6). As abasic DNA can be repaired through the BER pathway (7), we hypothesized FEN1 might be functionally involved in a long-patch BER response following the

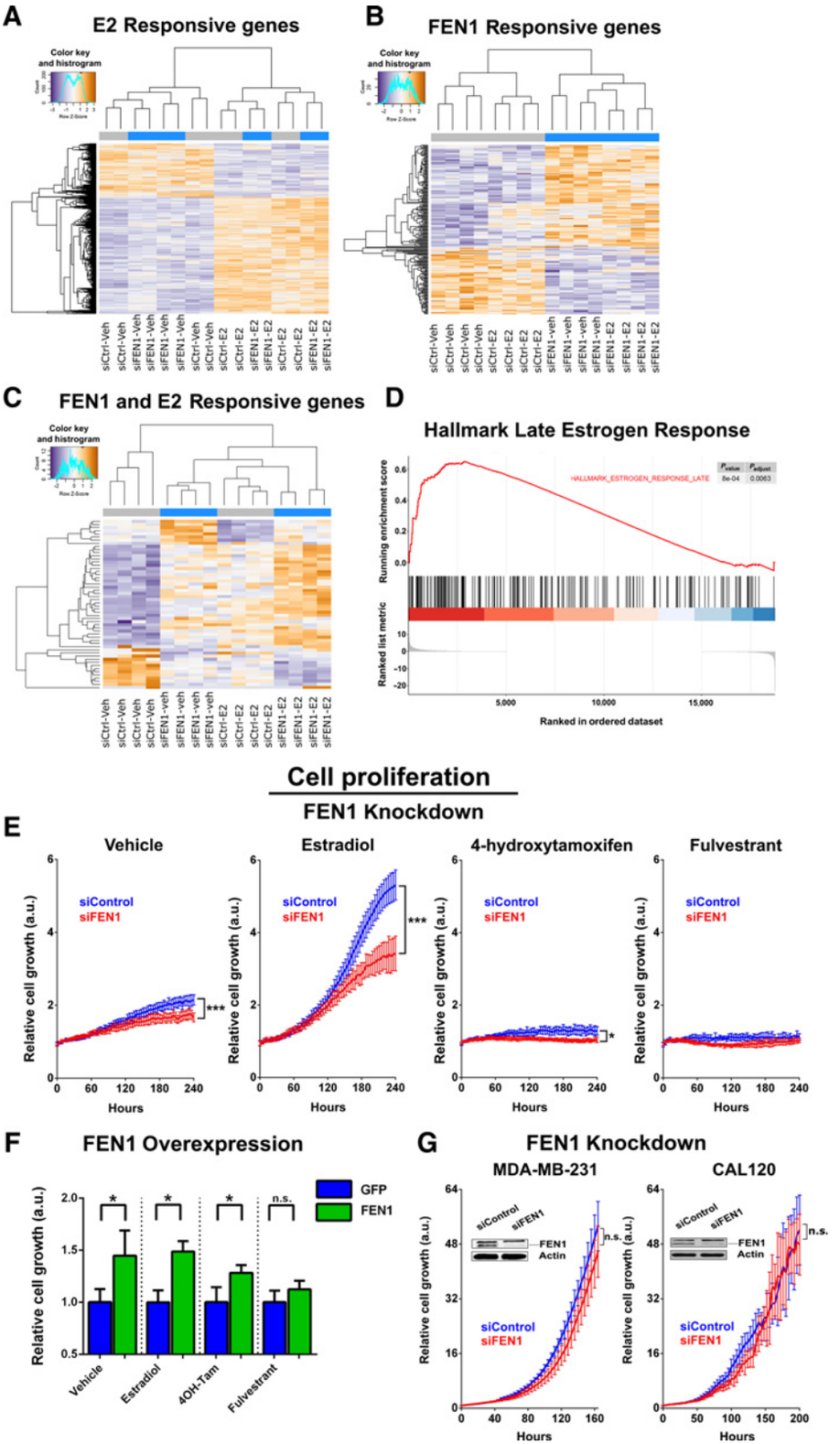

Figure 3.

FEN1 impacts ERα-mediated transcription and proliferation. **A,** Heatmap of the differentially expressed genes in E2 versus vehicle treatment. Depicted are four biological replicates of siControl (gray bar) and siFEN1 (blue bar) cells treated with vehicle or E2. **B,** As in **A**, but now the differentially expressed genes in siFEN1 versus siControl are depicted. **C,** As in **A**, but now genes differentially expressed in both conditions are depicted. **D,** GSEA for Hallmark Estrogen Response Late genes. Shown is ranking metric using the $\log_2FC^*$-$\log_{10}$ P value. See also Supplementary Fig. S3A. **E,** Relative cell proliferation (y-axis) over time (x-axis) of MCF7 cells treated with vehicle, E2, tamoxifen or fulvestrant. Cells were transfected with control siRNA (blue) or siFEN1 (red). Relative growth was normalized over the number of cells at timepoint zero. Shown is a representative experiment of three biological replicates. $N = 6$ with mean ± SD with Student t test at last time point. See also Supplementary Fig. S3B and SC. **F,** Relative cell proliferation of MCF7 cells treated with vehicle, E2, tamoxifen or fulvestrant. Cells were transfected with exogenous FEN1 (green) or GFP control (blue). Cell growth was normalized over GFP control after 150 hours of growth. Shown is a representative experiment of three biological replicates. $N = 6$ with mean ± SD. **G,** As in **E**, but now MDA-MB-231 and CAL120 ERα-negative cells were grown in full medium. FEN1 and actin protein levels as assessed by Western blot analysis are depicted. Shown are representative experiments of two biological replicates. $N = 6$ with mean ± SD. *, $P < 0.05$; ***, $P < 0.001$; n.s., nonsignificant.

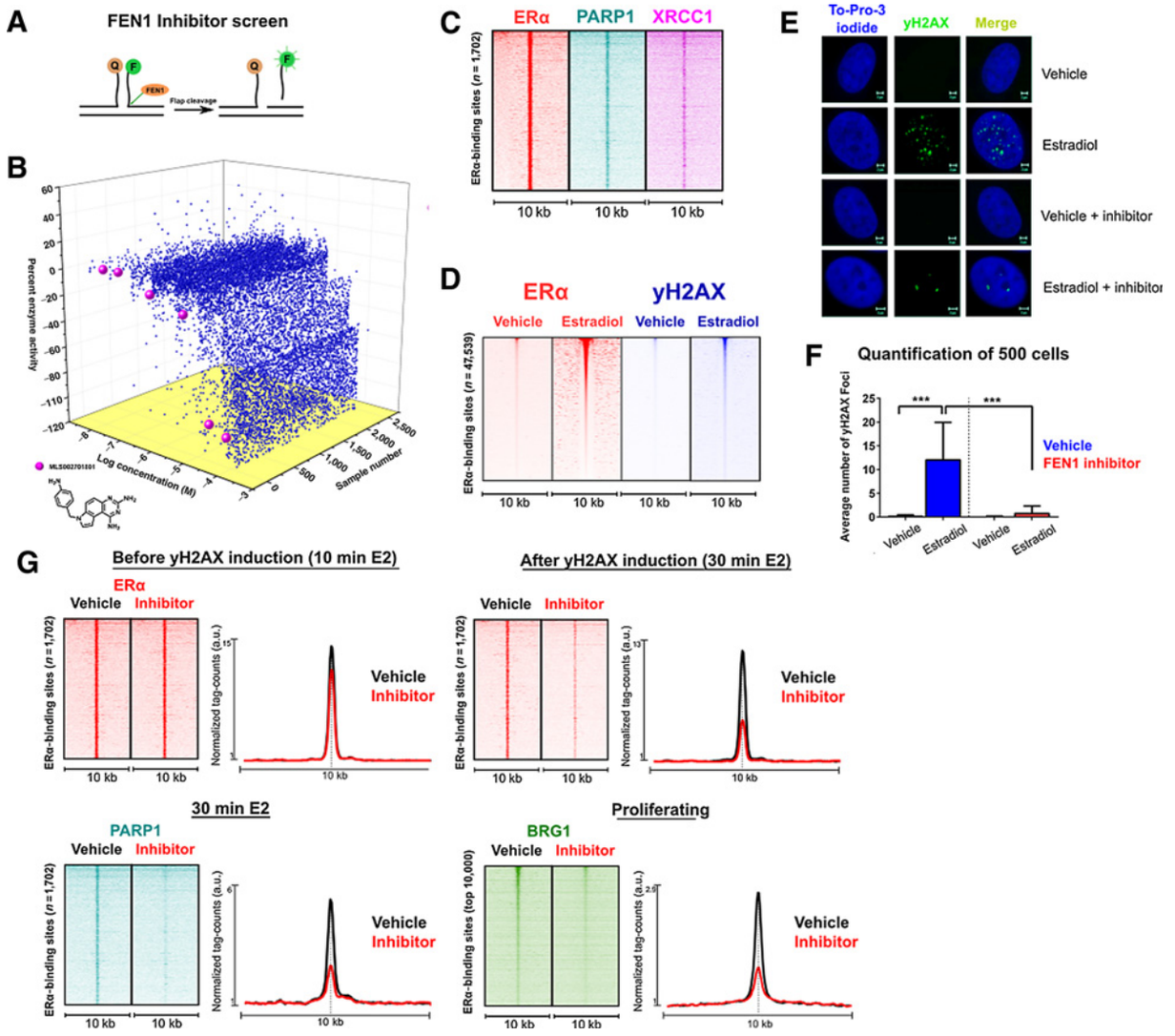

Figure 4.

FEN1 inhibitor screen and the role of FEN1 in ERα activity. **A,** Fluorescence-based assay used to assess flap-cleaving by FEN1. A double-stranded DNA flap substrate containing two tags, a fluorophore-donor (6-TAMRA) and a fluorophore-quencher (BHQ2), was exposed to FEN1 protein in the presence or absence of small-molecule compounds. Upon flap-cleavage the DNA product containing the fluorophore was released, resulting in measurable fluorescence signal. **B,** Concentration response profile of the 2,485 compounds found active as FEN1 inhibitors, identifying MLS002701801 (FENi#2; purple dot) as our top hit. For each compound, the concentration (log) and the percentage of altered FEN1 enzyme activity is depicted. See also Supplementary Table S3 and Supplementary Fig. S4A–S4C. **C,** Heatmap visualizing ranked binding events of ERα (red), PARP1 (dark cyan), and XRCC1 (purple) at ERα-binding sites. Hormone-deprived cells where treated with E2 for 10 (ERα and XRCC1) or 30 minutes (PARP1). All binding events at ERα-bound regions after 10 minutes of E2 were analyzed, vertically aligned, and centered at the center of the peak, with a 10 kb window. See also Supplementary Fig. S4D. **D,** As in **C**, but now binding events of ERα (red) and γH2AX (blue) at ERα-binding sites under vehicle or E2 conditions are visualized. Peaks were sorted on ERα intensity. See also Supplementary Fig. S4E and S4F. **E,** Induction of γH2AX-foci by E2 stimulation as visualized through immunofluorescence. Hormone-deprived cells where treated with ethanol or E2 for 15 minutes, with or without FEN1 inhibitor. Shown is a representative cell stained for γH2AX (green). To-Pro-3-iodide was used to visualize the nucleus (blue). Scale bar, 2 μm. **F,** The average number of γH2AX foci per cell as quantified in 500 cells. Shown is a representative experiment of two biological replicates. $N = 500$ with mean ± SD. See also Supplementary Fig. S4G. **F,** Top left, heatmap visualizing ranked binding events of ERα (red) at ERα sites. Hormone-deprived cells where pretreated with a vehicle or FEN1 inhibitor and subsequently stimulated with E2 for 10 minutes. All binding events at ERα sites after 10 minutes of E2 were analyzed, vertically aligned, and centered at the center of the peak, with a 10 kb window. Normalized tag counts are plotted, showing average signal intensity. Top right, as in top left, but now ERα-binding sites were analyzed for cells stimulated with E2 for 30 minutes. Bottom left, as in top left, but now PARP1 binding sites were analyzed for cells stimulated with E2 for 30 minutes. Bottom right, as in top left, but now BRG1 binding sites were analyzed for proliferating cells. See also Supplementary Fig. S4H. ***, $P < 0.001$.

formation of abasic sites, thereby regulating ERα activity. In agreement with a BER response near ERα-binding sites, we observed BER-members XRCC1 and PARP1 (7), to bind these genomic regions (**Fig. 4C**; Supplementary Fig. S4D), with PARP1 being described previously as coregulator of ERα (43). The APOBEC3B induced C-to-U modifications were shown to ultimately give rise to γH2AX formation at ERα sites (6), as assessed by ChIP-seq (**Fig. 4D**; Supplementary Fig. S4E and S4F). This γH2AX-induction was validated

by immunofluorescence, where 15 minutes of E2 stimulation induced γH2AX foci (**Fig. 4E** and **F**). FEN1 inhibition through 100 nmol/L FENi#2 blocked this E2-induced γH2AX-formation (**Fig. 4E** and **F**; Supplementary Fig. S4G) and could not be explained by lower ERα-chromatin interactions at time points preceding DNA damage (10 minutes after E2 stimulation; **Fig. 4G**; Supplementary Fig. S4H). Interestingly, when assessing ERα and PARP1 binding after 30 minutes of E2 stimulation, which is after the γH2AX induction found at 10′, FEN1 inhibition did decrease ERα and PARP1 chromatin binding (**Fig. 4G**; Supplementary Fig. S4H), which suggests that FEN1 perturbation effects on ERα binding only occur after the moment of γH2AX formation (10 minutes after E2 induction). In line with the known role of γH2AX in promoting chromatin remodeling (44), FEN1 inhibition decreased both γH2AX formation and recruitment of BRG1; the catalytic subunit of the SWI/SNF chromatin-remodeling complex (**Fig. 4G**; Supplementary Fig. S4H; ref. 44), which chromatin interactions overlapped ERα binding sites. Altogether this indicates that FEN1 plays a functional role during the induction of γH2AX and subsequent ERα and coregulator binding capacity.

An additional aspect of FEN1's regulatory role in ERα activity was found in the E2-induced proteasomal degradation of ERα (45). Herein, FEN1 inhibition enhanced E2-induced ERα degradation (Supplementary Fig. S4I), while pretreatment with proteasome inhibitor MG132 prevented this FENi#2-induced reduction of ERα-chromatin interactions (Supplementary Fig. S4I). This together with the observation that ERα-chromatin interactions were not affected by FEN1 inhibition until the moment of γH2AX induction (**Fig. 4G**; Supplementary Fig. S4H), favors a model wherein FEN1 regulates ERα-chromatin binding by preventing E2-induced proteasomal degradation.

Cumulatively, we identify FENi#2 as a potent and specific FEN1 inhibitor, and demonstrate that FEN1 regulates ERα activity through the functional formation of γH2AX, and subsequent BRG1 recruitment, and can regulate ERα-chromatin interactions by inhibiting proteasome-mediated degradation. In addition, we provide evidence that additional BER-members (PARP1 and XRCC1) are also present at sites of ERα binding.

FEN1 inhibition as novel drug option in tamoxifen-resistant breast cancer

Because tamoxifen-resistant cell lines (13) and tumors (46) still require ERα function, an alternative mode of blocking ERα action through FEN1 inhibition would have strong clinical potential.

To assess this, we investigated the effect of FENi#2 on ERα binding and induced gene expression. First, the optimal time point of ERα-chromatin interactions after E2 treatment was determined, with 30 minutes of E2 stimulation resulting in maximum detection of ERα-chromatin interactions (**Fig. 5A**). Overnight pretreatment with 100 nmol/L FENi#2 significantly inhibited these E2-induced ERα-chromatin interactions and ERα-driven gene transcription (**Fig. 5B**), analogous to siFEN1 (**Fig. 2**). This inhibition of ERα activity by FENi#2 showed a notable overlap with siFEN1, both in reduced cell growth as in ERα-binding perturbation (Supplementary Fig. S5A and S5B). In the absence of E2, ERα protein levels were unaffected by FENi#2 (Supplementary Fig. S5C), indicating decreased ERα-chromatin interactions and gene transcription were not due to reduced initial amounts of ERα protein.

Colony formation assays were performed for a panel of human breast cancer cell lines: (a) MCF7 and T47D (ERα+), (b) MCF7-T and TAMR [tamoxifen-resistant MCF7 derivatives (12, 13)], and (c) BT-20 and CAL-120 (ERα−). Cells were treated with increasing concentrations of FENi#2 in the presence or absence of tamoxifen (**Fig. 5C** and **D**), confirming tamoxifen responsiveness of the sensitive cell lines (**Fig. 5C** and **D**). Proliferation of MCF7 and T47D cells was inhibited in a dose-dependent manner with IC_{50} values of 69 and 78 nmol/L of the inhibitor, respectively (Supplementary Table S4). In contrast, sensitivity to FENi#2 for ERα-negative cell lines BT-20 and CAL120 was limited, with an IC_{50} of 314 nmol/L in BT20, while not reaching 50% inhibition in CAL120 cells. Interestingly, tamoxifen-resistant MCF7 derivatives showed enhanced sensitivity to FEN1 inhibition in relation to the parental cells (IC_{50} = 29 nmol/L for both tamoxifen-resistant cell lines).

To validate the efficacy of FEN1 inhibition in ERα-positive breast cancer, we used *ex vivo* primary ERα-positive tumor cultures (i.e., explants; refs. 30, 31) in the presence or absence of compound FENi#2. Tumors were cut into small pieces and randomized between vehicle, FEN1 inhibitor or tamoxifen treatments and cultured for 3–6 days on gelatin sponges, allowing sustained tissue architecture and viability (31). Explants were stained for cell proliferation marker Ki67 and scored by a pathologist. Upon FEN1 inhibition, all four tumor explants demonstrated reduced proliferation (Ki67; **Fig. 5E** and **F**). For 3 of 4 explants, sufficient material was available for testing tamoxifen in this setting, demonstrating comparable reductions in Ki67 signal (Supplementary Fig. S5D).

Taken together, we show that pharmacologic inhibition of FEN1 efficiently blocks ERα-driven tumor cell proliferation, with enhanced potency in tamoxifen-resistant cells. As FEN1 perturbation inhibits primary tumor tissue growth, we demonstrate therapeutic potential of our FEN1 inhibitor in the treatment of ERα-positive cancer.

Discussion

Several multigene prognostic classifiers have been reported that stratify patients with breast cancer on outcome (47). Most of these classifiers lack biological insights regarding the drivers of tumor progression. Here, we refined a 111-gene classifier to a single gene predictor of disease outcome, revealing a drug target with clinical potential in the treatment of tamoxifen-resistant breast tumors. We identified FEN1 as a predictive marker for tamoxifen resistance in clinical specimens, with potential for outcome-prediction exclusive in ERα-positive breast cancers. Before any clinical implication of FEN1 as a predictive marker however, the predictive versus prognostic potential of FEN1 needs to be validated in an independent second randomized clinical trial of tamoxifen versus placebo. Of note, previous work from Abdel-Fatah and colleagues describes FEN1 protein levels to correlate with a poor outcome in ERα-positive as well as in patients with ERα-negative breast cancer (11). This discrepancy might be best explained by the use of different antibodies used for IHC and the fact that Abdel-Fatah and colleagues also reported cytoplasmic staining (11), which was absent in our stainings. Our observation that FEN1 has predictive potential in ERα-positive cases is in line with our cell proliferation analyses, where perturbation of FEN1 was only effective in ERα-positive cell lines, while yielding no detectable effects in ERα-negative cells.

Accumulating evidence repositions DNA repair factors as coactivators of transcription, among other in facilitating chromatin remodeling (5). Chromatin remodeling at ERα-binding regions can be initiated by BRG1 (48), the recruitment of which is promoted by γH2AX (44). Failure to induce γH2AX-signaling at ERα regions diminished BRG1 recruitment (6), implicating ERα-induced γH2AX as facilitator of chromatin remodeling. We found FEN1 to be critically involved in this process and can thereby regulate BRG1 recruitment,

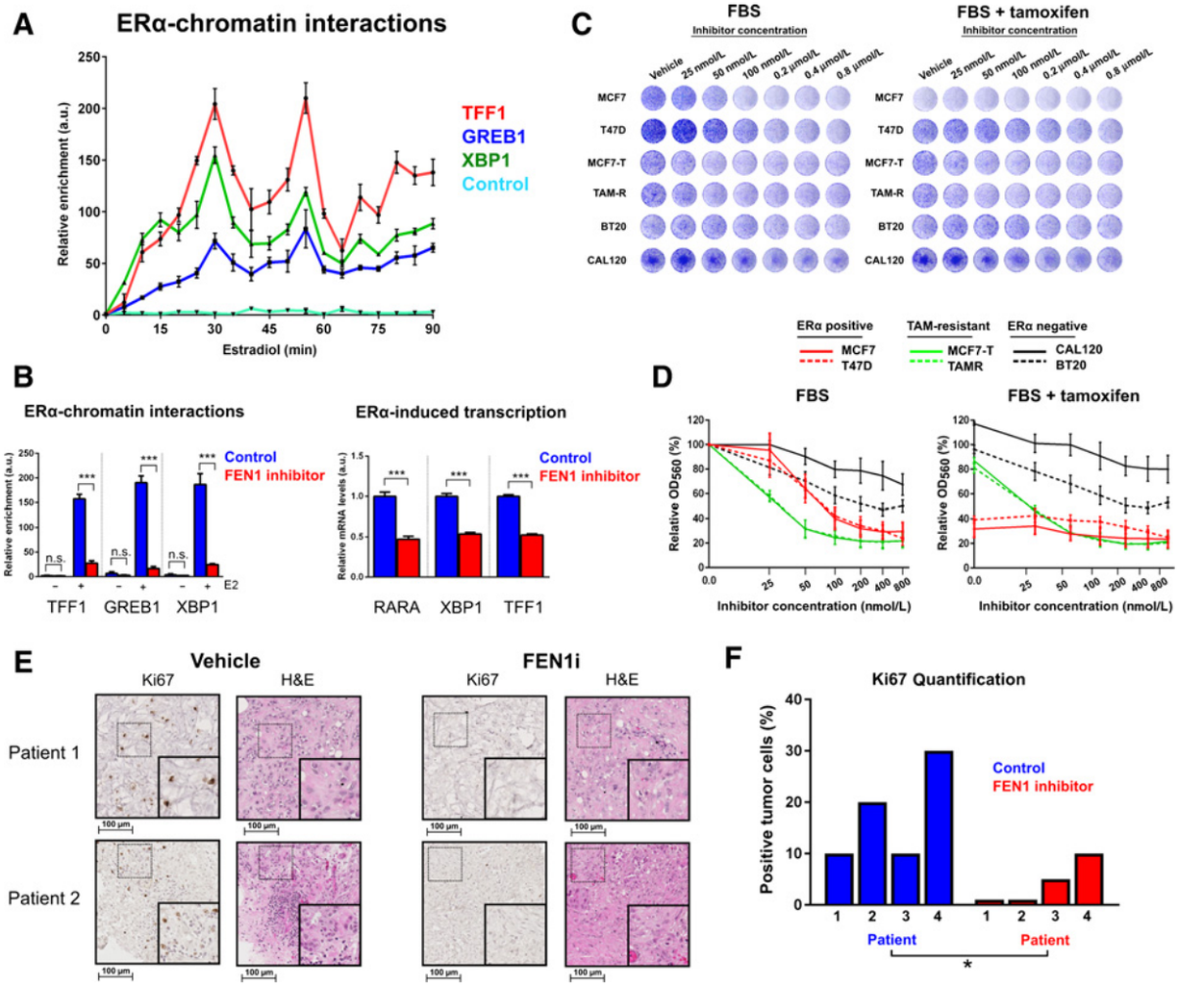

Figure 5.

Small molecule–mediated inhibition of FEN1 blocks ERα action and prevents cell proliferation. **A,** ERα ChIP-qPCR analyses of hormone-deprived cells treated for 90 minutes with E2 using 5-minute intervals. Three positive regions for ERα binding were assessed (TFF1, GREB1, and XBP1) and one known negative region (Neg control). Data are normalized over t = 0. $N = 4$ with mean ± SD. **B,** Left, ERα ChIP-qPCR analyses of hormone-deprived cells pretreated with vehicle or FEN1 inhibitor prior to 30 minutes of E2 treatment. Signals were normalized over control genomics regions. Shown is a representative experiment of two biological replicates. $N = 4$ with mean ± SD. Right, relative mRNA levels of RARA, XBP1, and TFF1 with or without FEN1 inhibitor. TBP and UBC were used as control. Shown is a representative experiment of two biological replicates. $N = 4$ with mean ± SD. **C,** Colony formation analyses for breast cancer cell lines MCF7 and T47D (ERα+), MCF7-T and TAMR (tamoxifen-resistant MCF7 derivatives), and BT-20 and CAL-120 (ERα−). Cells were treated with increasing concentrations of FEN1 inhibitor in the presence or absence of tamoxifen. Representative experiment is shown of at least four biological replicates. **D,** Relative quantified crystal violet staining (OD_{560}) of colony formation assay depicted in **C**. Shown are mean values of at least four biological experiments where all OD_{560} data were normalized to vehicle-treated FBS. Error bars, SEM. See also Supplementary Table S4. **E,** *Ex vivo* primary human ERα-positive tumor cultures in the presence or absence of 200 nmol/L FEN1 inhibitor. Explants were fixed and stained for Ki67 and hematoxylin and eosin (H&E). Shown are representative tumor regions for two patients with digital zoom in the lower right corner. **F,** Indication of the percentage of Ki67-positive tumor cells in tumor explants cultured in the presence or absence of FEN1 inhibitor. Paired Student *t* test was used to assess the difference between treatment groups. See also Supplementary Fig. S5D. *, $P < 0.05$; ***, $P < 0.001$; n.s., nonsignificant.

and ultimately enable transcription. Interestingly enough, we observed that the decrease in ERα chromatin binding by FEN1 inhibition only seem to occur after the moment of γH2AX-formation (**Fig. 4G**). Besides BRG1, we demonstrate that SRC3 and p300 recruitment to ERα transcriptional complex is also dependent on FEN1. In addition, FEN1 inhibition enhanced E2-induced ERα degradation, mediated by proteasomal activity (45). Consequently, this favors a model wherein, along with being crucial for cofactor recruitment (as exemplified by SRC3, p300, and BRG1), FEN1 can also alter ERα's activity by regulating the stability of its chromatin binding after activation by E2.

Transcription-coupled degradation of the ERα is well known for many years (45, 49–51), but still not fully understood. Interestingly, inhibiting FEN1 resulted in a ligand-driven loss of ERα chromatin interactions, which associates with a loss of ERα protein levels, suggesting that FEN1 inhibition could potentially uncouple transcriptional events from proteasome-mediated degradation of the receptor.

Further studies should be aimed to elucidate this mechanism, and determine how FEN1 is mechanistically involved in this.

Small molecule–mediated inhibition of FEN1 functionally abrogated ERα activity and ultimately blocked human tumor explant proliferation. With an inhibitor effective in the nanomolar range, we illustrate that FEN1 inhibition might yield a promising novel therapy for ERα-positive breast cancer. While FEN1 inhibition has been described before, it has mainly been linked to chemosensitization (52, 53) or as a part of synthetic lethal interactions (40, 54), but not as an effective therapeutic strategy on its own (42). Although it is widely accepted that most small-molecule inhibitors are not truly specific for their targets, including most clinically applied small molecules (55), our FEN1 inhibitor was inactive in almost all of the 150 additional protein assays we investigated (Supplementary Fig. S4B; Supplementary Table S3). Even though the effect of siFEN1 and the inhibitor were very similar, there could still be some off-target effects making additional chemical matter refinements required for further clinical development of FEN1 targeting in breast cancer. Here we report the first effective single-agent application of FEN1 inhibition by specifically targeting ERα-positive breast cancer. Most importantly, tamoxifen-resistant cell lines showed an increased sensitivity for FEN1 blockade; a feature that could possibly be exploited in the treatment of advanced breast cancer, thereby providing a novel targeted therapy in case of tamoxifen resistance.

Disclosure of Potential Conflicts of Interest

No potential conflicts of interest were disclosed.

Authors' Contributions

Conception and design: K.D. Flach, W. Zwart

Development of methodology: K.D. Flach, M. Periyasamy, D. Dorjsuren, A. Simeonov

Acquisition of data (provided animals, acquired and managed patients, provided facilities, etc.): K.D. Flach, A. Jadhav, T.E. Hickey, M. Opdam, H. Patel, D.M. Wilson III, M. Donaldson Collier, S. Prekovic, M. Nieuwland, J. Wesseling, S.C. Linn, W.D. Tilley, A. Simeonov, S. Ali

Analysis and interpretation of data (e.g., statistical analysis, biostatistics, computational analysis): K.D. Flach, A. Jadhav, D. Dorjsuren, J.C. Siefert, M. Opdam, S. Canisius, R.J.C. Kluin, A.V. Zakharov, L.F.A. Wessels, W.D. Tilley, S. Ali

Writing, review, and/or revision of the manuscript: K.D. Flach, J.C. Siefert, T.E. Hickey, D.M. Wilson III, J. Wesseling, L.F.A. Wessels, S.C. Linn, A. Simeonov, S. Ali, W. Zwart

Administrative, technical, or material support (i.e., reporting or organizing data, constructing databases): K.D. Flach, J. Wesseling

Study supervision: A. Simeonov, W. Zwart

Acknowledgments

The authors thank Ron Kerkhoven from the NKI Genomics Core Facility. The authors thank Sheila Stewart (Department of Cell Biology and Physiology, Washington University, St. Louis, MO) for providing pShuttle-FEN1hWT and pShuttle-D181A, Robert Nicholson (Cardiff School of Pharmacy and Pharmaceutical Science, Cardiff University, United Kingdom) for providing the TAM-R cells, Kenneth Nephew (Indiana University, School of Medicine, Bloomington, IN) for providing MCF7-T cells. The authors thank Hongmao Sun and David Maloney (National Center for Advancing Translational Sciences, NIH, Bethesda, MD) for the additional design and analyses of the FEN1 HTS inhibitor screen and synthesis of required protein and reagents. This work was supported by the Dutch Cancer Society KWF, Netherlands Organization for Scientific Research (NWO), A Sister's Hope, the National Center for Advancing Translational Sciences, National Institutes of Health (R03 MH092154-01), National Institute on Aging, the National Health and Medical Research Council of Australia (ID 1084416; ID 20160711 to W.D. Tilley and T.E. Hickey), the Royal Adelaide Hospital Research Foundation and the Cancer Australia/National Breast Cancer Foundation (ID CA1043497).

The costs of publication of this article were defrayed in part by the payment of page charges. This article must therefore be hereby marked *advertisement* in accordance with 18 U.S.C. Section 1734 solely to indicate this fact.

Received July 17, 2019; revised January 30, 2020; accepted March 9, 2020; published first March 19, 2020.

References

1. Glass CK, Rose DW, Rosenfeld MG. Nuclear receptor coactivators. Curr Opin Cell Biol 1997;9:222–32.
2. Jordan VC, Murphy CS. Endocrine pharmacology of antiestrogens as antitumor agents. Endocr Rev 1990;11:578–610.
3. Shou J, Massarweh S, Osborne CK, Wakeling AE, Ali S, Weiss H, et al. Mechanisms of tamoxifen resistance: increased estrogen receptor-HER2/neu cross-talk in ER/HER2-positive breast cancer. J Natl Cancer Inst 2004;96:926–35.
4. Zwart W, Theodorou V, Kok M, Canisius S, Linn S, Carroll JS. Oestrogen receptor-co-factor-chromatin specificity in the transcriptional regulation of breast cancer. EMBO J 2011;30:4764–76.
5. Fong YW, Cattoglio C, Tjian R. The intertwined roles of transcription and repair proteins. Mol Cell 2013;52:291–302.
6. Periyasamy M, Patel H, Lai CF, Nguyen VT, Nevedomskaya E, Harrod A, et al. APOBEC3B-mediated cytidine deamination is required for estrogen receptor action in breast cancer. Cell Rep 2015;13:108–21.
7. Krokan HE, Bjoras M. Base excision repair. Cold Spring Harb Perspect Biol 2013;5:a012583.
8. Zheng L, Shen B. Okazaki fragment maturation: nucleases take centre stage. J Mol Cell Biol 2011;3:23–30.
9. Singh P, Yang M, Dai H, Yu D, Huang Q, Tan W, et al. Overexpression and hypomethylation of flap endonuclease 1 gene in breast and other cancers. Mol Cancer Res 2008;6:1710–7.
10. Schultz-Norton JR, Walt KA, Ziegler YS, McLeod IX, Yates JR, Raetzman LT, et al. The deoxyribonucleic acid repair protein flap endonuclease-1 modulates estrogen-responsive gene expression. Mol Endocrinol 2007;21:1569–80.
11. Abdel-Fatah TM, Russell R, Albarakati N, Maloney DJ, Dorjsuren D, Rueda OM, et al. Genomic and protein expression analysis reveals flap endonuclease 1 (FEN1) as a key biomarker in breast and ovarian cancer. Mol Oncol; 2014:8:1326–38.
12. Fan M, Yan PS, Hartman-Frey C, Chen L, Paik H, Oyer SL, et al. Diverse gene expression and DNA methylation profiles correlate with differential adaptation of breast cancer cells to the antiestrogens tamoxifen and fulvestrant. Cancer Res 2006;66:11954–66.
13. Knowlden JM, Hutcheson IR, Jones HE, Madden T, Gee JM, Harper ME, et al. Elevated levels of epidermal growth factor receptor/c-erbB2 heterodimers mediate an autocrine growth regulatory pathway in tamoxifen-resistant MCF-7 cells. Endocrinology 2003;144:1032–44.
14. Saharia A, Teasley DC, Duxin JP, Dao B, Chiappinelli KB, Stewart SA. FEN1 ensures telomere stability by facilitating replication fork re-initiation. J Biol Chem 2010;285:27057–66.
15. Hurtado A, Holmes KA, Ross-Innes CS, Schmidt D, Carroll JS. FOXA1 is a key determinant of estrogen receptor function and endocrine response. Nat Genet 2011;43:27–33.
16. Giresi PG, Lieb JD. Isolation of active regulatory elements from eukaryotic chromatin using FAIRE (Formaldehyde Assisted Isolation of Regulatory Elements). Methods 2009;48:233–9.
17. Jansen MP, Knijnenburg T, Reijm EA, Simon I, Kerkhoven R, Droog M, et al. Hallmarks of aromatase inhibitor drug resistance revealed by epigenetic profiling in breast cancer. Cancer Res 2013;73:6632–41.
18. Zhang Y, Liu T, Meyer CA, Eeckhoute J, Johnson DS, Bernstein BE, et al. Model-based analysis of ChIP-Seq (MACS). Genome Biol 2008;9:R137.

19. Kumar V, Muratani M, Rayan NA, Kraus P, Lufkin T, Ng HH, et al. Uniform, optimal signal processing of mapped deep-sequencing data. Nat Biotechnol 2013;31:615–22.
20. Ye T, Krebs AR, Choukrallah MA, Keime C, Plewniak F, Davidson I, et al. seqMINER: an integrated ChIP-seq data interpretation platform. Nucleic Acids Res 2011;39:e35.
21. Lopez-Garcia J, Periyasamy M, Thomas RS, Christian M, Leao M, Jat P, et al. ZNF366 is an estrogen receptor corepressor that acts through CtBP and histone deacetylases. Nucleic Acids Res 2006;34:6126–36.
22. Kok M, Holm-Wigerup C, Hauptmann M, Michalides R, Stal O, Linn S, et al. Estrogen receptor-alpha phosphorylation at serine-118 and tamoxifen response in breast cancer. J Natl Cancer Inst 2009;101:1725–9.
23. Kok M, Linn SC, Van Laar RK, Jansen MP, van den Berg TM, Delahaye LJ, et al. Comparison of gene expression profiles predicting progression in breast cancer patients treated with tamoxifen. Breast Cancer Res Treat 2009;113: 275–83.
24. Michalides R, van Tinteren H, Balkenende A, Vermorken JB, Benraadt J, Huldij J, et al. Cyclin A is a prognostic indicator in early stage breast cancer with and without tamoxifen treatment. Br J Cancer 2002;86:402–8.
25. Beelen K, Opdam M, Severson TM, Koornstra RH, Vincent AD, Wesseling J, et al. Phosphorylated p-70S6K predicts tamoxifen resistance in postmenopausal breast cancer patients randomized between adjuvant tamoxifen versus no systemic treatment. Breast Cancer Res 2014;16:R6.
26. Tibshirani R, Hastie T, Narasimhan B, Chu G. Diagnosis of multiple cancer types by shrunken centroids of gene expression. Proc Natl Acad Sci U S A 2002;99: 6567–72.
27. Friedman J, Hastie T, Tibshirani R. Regularization paths for generalized linear models via coordinate descent. J Stat Softw 2010;33:1–22.
28. Loi S, Haibe-Kains B, Desmedt C, Lallemand F, Tutt AM, Gillet C, et al. Definition of clinically distinct molecular subtypes in estrogen receptor-positive breast carcinomas through genomic grade. J Clin Oncol 2007;25: 1239–46.
29. Buffa FM, Camps C, Winchester L, Snell CE, Gee HE, Sheldon H, et al. microRNA-associated progression pathways and potential therapeutic targets identified by integrated mRNA and microRNA expression profiling in breast cancer. Cancer Res 2011;71:5635–45.
30. Dean JL, McClendon AK, Hickey TE, Butler LM, Tilley WD, Witkiewicz AK, et al. Therapeutic response to CDK4/6 inhibition in breast cancer defined by *ex vivo* analyses of human tumors. Cell Cycle 2012;11:2756–61.
31. Mohammed H, Russell IA, Stark R, Rueda OM, Hickey TE, Tarulli GA, et al. Progesterone receptor modulates ERalpha action in breast cancer. Nature 2015; 523:313–7.
32. Dorjsuren D, Kim D, Maloney DJ, Wilson DM III, Simeonov A. Complementary non-radioactive assays for investigation of human flap endonuclease 1 activity. Nucleic Acids Res 2011;39:e11.
33. Inglese J, Auld DS, Jadhav A, Johnson RL, Simeonov A, Yasgar A, et al. Quantitative high-throughput screening: a titration-based approach that efficiently identifies biological activities in large chemical libraries. Proc Natl Acad Sci U S A 2006;103:11473–8.
34. Michael S, Auld D, Klumpp C, Jadhav A, Zheng W, Thorne N, et al. A robotic platform for quantitative high-throughput screening. Assay Drug Dev Technol 2008;6:637–57.
35. Yasgar A, Shinn P, Jadhav A, Auld D, Michael S, Zheng W, et al. Compound management for quantitative high-throughput screening. JALA 2008;13: 79–89.
36. Jadhav A, Ferreira RS, Klumpp C, Mott BT, Austin CP, Inglese J, et al. Quantitative analyses of aggregation, autofluorescence, and reactivity artifacts in a screen for inhibitors of a thiol protease. J Med Chem 2010;53:37–51.
37. Curtis C, Shah SP, Chin SF, Turashvili G, Rueda OM, Dunning MJ, et al. The genomic and transcriptomic architecture of 2,000 breast tumours reveals novel subgroups. Nature 2012;486:346–52.
38. Beelen K, Zwart W, Linn SC. Can predictive biomarkers in breast cancer guide adjuvant endocrine therapy? Nat Rev Clin Oncol 2012:9:529–41.
39. Zheng L, Jia J, Finger LD, Guo Z, Zer C, Shen B. Functional regulation of FEN1 nuclease and its link to cancer. Nucleic Acids Res 2011;39:781–94.
40. van Pel DM, Barrett IJ, Shimizu Y, Sajesh BV, Guppy BJ, Pfeifer T, et al. An evolutionarily conserved synthetic lethal interaction network identifies FEN1 as a broad-spectrum target for anticancer therapeutic development. PLoS Genet 2013;9:e1003254.
41. Tumey LN, Bom D, Huck B, Gleason E, Wang J, Silver D, et al. The identification and optimization of a N-hydroxy urea series of flap endonuclease 1 inhibitors. Bioorg Med Chem Lett 2005;15:277–81.
42. Exell JC, Thompson MJ, Finger LD, Shaw SJ, Debreczeni J, Ward TA, et al. Cellularly active N-hydroxyurea FEN1 inhibitors block substrate entry to the active site. Nat Chem Biol 2016;12:815–21.
43. Zhang F, Wang Y, Wang L, Luo X, Huang K, Wang C, et al. Poly(ADP-ribose) polymerase 1 is a key regulator of estrogen receptor alpha-dependent gene transcription. J Biol Chem 2013;288:11348–57.
44. Lee HS, Park JH, Kim SJ, Kwon SJ, Kwon J. A cooperative activation loop among SWI/SNF, gamma-H2AX and H3 acetylation for DNA double-strand break repair. EMBO J 2010;29:1434–45.
45. Nawaz Z, Lonard DM, Dennis AP, Smith CL, O'Malley BW. Proteasome-dependent degradation of the human estrogen receptor. Proc Natl Acad Sci U S A 1999;96:1858–62.
46. Robinson DR, Wu YM, Vats P, Su F, Lonigro RJ, Cao X, et al. Activating ESR1 mutations in hormone-resistant metastatic breast cancer. Nat Genet 2013;45: 1446–51.
47. Dai X, Li T, Bai Z, Yang Y, Liu X, Zhan J, et al. Breast cancer intrinsic subtype classification, clinical use and future trends. Am J Cancer Res 2015;5:2929–43.
48. DiRenzo J, Shang Y, Phelan M, Sif S, Myers M, Kingston R, et al. BRG-1 is recruited to estrogen-responsive promoters and cooperates with factors involved in histone acetylation. Mol Cell Biol 2000;20:7541–9.
49. Callige M, Richard-Foy H. Ligand-induced estrogen receptor alpha degradation by the proteasome: new actors? Nucl Recept Signal 2006;4:e004.
50. Tecalco-Cruz AC, Ramirez-Jarquin JO. Mechanisms that increase stability of estrogen receptor alpha in breast cancer. Clin Breast Cancer 2017;17:1–10.
51. Maggi A. Liganded and unliganded activation of estrogen receptor and hormone replacement therapies. Biochim Biophys Acta 2011;1812:1054–60.
52. He L, Zhang Y, Sun H, Jiang F, Yang H, Wu H, et al. Targeting DNA flap endonuclease 1 to impede breast cancer progression. EBioMedicine 2016;14: 32–43.
53. Panda H, Jaiswal AS, Corsino PE, Armas ML, Law BK, Narayan S. Amino acid Asp181 of 5'-flap endonuclease 1 is a useful target for chemotherapeutic development. Biochemistry 2009;48:9952–8.
54. McManus KJ, Barrett IJ, Nouhi Y, Hieter P. Specific synthetic lethal killing of RAD54B-deficient human colorectal cancer cells by FEN1 silencing. Proc Natl Acad Sci U S A 2009;106:3276–81.
55. Klaeger S, Heinzlmeir S, Wilhelm M, Polzer H, Vick B, Koenig PA, et al. The target landscape of clinical kinase drugs. Science 2017;358. DOI: 10.1126/science.aan4368.